Measurement of Radiative Non-equilibrium for Air Shocks Between 7-9 km/s

Brett A. Cruden[1], Aaron M. Brandis[2]
AMA, Inc. at NASA Ames Research Center, Moffett Field, CA, 94035

This paper describes a recent characterization of non-equilibrium for shock speeds between 7 and 9 km/s in the NASA Ames Electric Arc Shock Tube (EAST) Facility. Data is spectrally resolved from 190-1450 nm and spatially resolved behind the shock front. Comparisons are made to DPLR/NEQAIR simulations using different modeling options and recommendations for future study are made based on these comparisons.

I. Introduction

In recent years, extensive campaigns have been conducted to measure radiation in air shocks at velocities from 9-15 km/s.[1] However, little recent data exists characterizing the radiation characteristics below this velocity range. Although the radiative heat flux magnitude in this velocity region is relatively small, around 10% of the radiative heat load may originate from velocities less than 9 km/s for lunar return. For entries from low earth orbit, it comprises the entirety of radiative heating. Therefore, a test series has been undertaken in the EAST facility to characterize this range, the results of which are reported here. Experiments were undertaken in the 7-9 km/s velocity range, at six different freestream pressures from 0.01-0.70 Torr. Simulations of these experiments were carried out with the DPLR and NEQAIR codes with 12 different modelling options. The amount of data (measured and simulated) is voluminous, so that a subset of results is presented in order to draw general conclusions about the state of predictive modelling.

II. Experiment

The EAST facility has been described in detail in previous work [2]. A 1.2 MJ, 40 kV capacitor bank drives one of two shock tubes. The first is a 60.33 cm inner diameter stainless steel tube, intended for testing at low density, and the second is a 10.16 cm aluminum tube which has been extensively utilized in high velocity testing in recent years. The observation section is located 21.4 m downstream of the diaphragm in the 60 cm tube and 7.9 m downstream in the 10 cm tube. The radiance is imaged axially onto one of four spectrometers, producing spectrally and spatially resolved radiance data in each test. On the 60 cm tube, two spectrometers are simultaneously in use, while four spectrometers are used simultaneously on the 10 cm tube. Between these spectrometers, radiance is measured from 190-540 nm and/or 480-1450 nm with each test.

Tests in the 60 cm tube were conducted with initial pressures of 0.01, 0.05 and 0.14 Torr, while the 10 cm tube was employed at pressures of 0.14, 0.30, 0.50 and 0.70 Torr. The velocities spanned 6.8-9.2 km/s, with higher velocities generally being tested at lower pressures. A total of 51 tests were conducted, 33 of which were performed in the 24" tube. Of these tests, 44 were deemed to have acceptable data quality. For each of the six pressures examined, one representative test is selected for further analysis. In order to provide analysis at all wavelengths and on both tubes, this requires 10 shots to be analyzed. The conditions of the shots are shown in Table I below.

[1] Sr. Research Scientist, Aerothermodynamics Branch. Associate Fellow AIAA. Contact: brett.a.cruden@nasa.gov
[2] Sr. Research Scientist, Aerothermodynamics Branch. Senior Member AIAA.

Table I. Shot Conditions presented in this work

Shot No	Velocity (km/s)	Pressure (torr)	Range (nm)	Tube Diameter (cm)
15	8.18	0.01	190-500	60.33
32	8.57	0.01	500-1450	60.33
8	8.62	0.05	190-500	60.33
24	8.87	0.05	500-1450	60.33
20	8.29	0.14	190-500	60.33
22	8.36	0.14	500-1450	60.33
38	8.33	0.14	190-1450	10.16
42	8.09	0.3	190-1450	10.16
46	7.71	0.5	190-1450	10.16
50	7.34	0.7	190-1450	10.16

III. Simulation

In order to simulate these results, it is assumed that the shock tube measurements show similarity to the stagnation line over a blunt body. A 3-m sphere is simulated using DPLR v4.04.0.[3] The stagnation line is then passed to NEQAIR15[4], which is run in "shock tube" mode (i.e. radiance calculated perpendicular to the line-of-sight direction) to create a radiation profile along the tube axis. In order to investigate the impact of different modeling choices on the radiance, different modeling options are explored. The options are summarized in Table II below.

Table II. Thermophysical Modeling Options Emloyed in this work

Modeling Option	Options		
Electron(ic) Energy	Te=Tt	Te=Tv	
Chemical Kinetics	Park 90 [5]	Park 93 [6]	Johnston 14 [7]
Impact Excitation	Park[5]	Huo[8]	

The first option involves how electron and electronic energy are accounted for within the context of the two-temperature model. Traditionally, DPLR has assumed energy stored in these modes to be determined by a combined translational-rotational-electronic temperature, with a separate temperature used to describe vibrational energy. In contrast, other codes such as LAURA[9] have assumed the vibrational and electronic modes to be lumped. The traditional DPLR approach poses a difficulty for radiation solutions as the large translational temperatures obtained in thermal non-equilibrium result in excessive radiation from electronic states. The solution had been to set the electronic temperature to the vibrational temperature when the DPLR stagnation line was parsed to the radiation code, even though it was inconsistent with the way the CFD solution was run. DPLR v4.04.0 now provides an option to simulate the energy partition with a lumped vibrational-electronic temperature, thus removing the need for the above workaround.

The second option is the chemical kinetic model used to produce the chemical non-equilibrium solution. Traditionally, the rates published in Park's 1990 text have been employed by NASA flight projects.[5] In 1993, Park published an update to these rates which is also run in this work.[6] The third chemistry model uses the rates employed by Johnston in 2014[7], which are the rates currently used with the LAURA CFD code. These rates are largely based on the work of Park, though some have been modified based on more recent studies. A summary of the differences in the three rate models is given in Table III. From the table it is seen that six rates were altered from Park90 to Park93 while Johnston employs ten different rates from Park90. An additional variation exists in the controlling temperature for associative ionization processes. It has long been standard practice in the two temperature model to use $\sqrt{TT_v}$ as the controlling temperature for dissociation reactions and T as the controlling temperature for other reactions. Reactions that involve electron impact might be expected to be controlled by T_e, however the existing formulation of DPLR does not allow this. A modified version of DPLR was run which allowed dissociative recombination (i.e. the reverse of associative ionization) to be controlled by T_e, and the impact of this modification is assessed.

Table III. Summary of reaction rate sources by kinetic rate model

Reaction	Park 90	Park 93[3]	Johnston 2014[4]
$N_2 + M \leftrightarrow 2N + M$	[5]	[5]	[5]
$O_2 + M \leftrightarrow 2O + M$	[5]	[5]	[5]
$NO + M \leftrightarrow N + O + M$	[5]	[5]	[10]
$N + e^- \leftrightarrow N^+ + 2e^-$	[6][5]	[6]	[6]
$O + e^- \leftrightarrow O^+ + 2e^-$	[5]	[5]	[5]
$N_2 + O \leftrightarrow NO + N$	[5]	[5]	[11]
$NO + O \leftrightarrow O_2 + N$	[5]	[5]	[12]
$N + O \leftrightarrow NO^+ + e^-$	[5]	[6]	[5]
$N + N \leftrightarrow N_2^+ + e$	[5]	[6]	[6]
$O + O \leftrightarrow O_2^+ + e$	[5]	[6]	[6]
$O^+ + N_2 \leftrightarrow N_2^+ + O$	[5]	[5]	[5]
$O^+ + NO \leftrightarrow N^+ + O_2$	[5]	[5][6]	[6]
$NO^+ + O_2 \leftrightarrow O_2^+ + NO$	[5]	[5]	[5]
$NO^+ + N \leftrightarrow N_2^+ + O$	[5]	[5]	[5]
$NO^+ + O \leftrightarrow N^+ + O_2$	[5]	[5]	[5]
$O_2^+ + N \leftrightarrow N^+ + O_2$	[5]	[5]	[5]
$O_2^+ + N_2 \leftrightarrow N_2^+ + O_2$	[5]	[5]	[5]
$NO^+ + N \leftrightarrow O^+ + N_2$	[5]	[5]	[5]
$NO^+ + O \leftrightarrow O_2^+ + N$	[5]	[5]	[5]
$N^+ + N_2 \leftrightarrow N_2^+ + N$	N/A	[6]	[6]
$O_2^+ + O \leftrightarrow O^+ + O_2$	N/A[7]	[6]	[6]
$N_2 + e \leftrightarrow N + N + e$	[5]	[6]	[13]
$O_2 + e \leftrightarrow O_2^+ + e$	N/A	N/A	[14]

The final variation examined within the NEQAIR code is the electron impact rates which determine the state populations in non-equilibrium (i.e. non-Boltzmann). The standard release of the NEQAIR code uses rates based upon the work of Park.[5] More recently, new rates for N, O and C have been calculated and compiled by Huo.[8] These rates are more similar to those utilized by the HARA code. These rates were converted to the NEQAIR input format for nitrogen atoms in order to evaluate the impact of these newer rates.

All together, there are $2 \times 3 \times 2$ options which makes for 12 different variations in modeling options. All 12 variants have been examined by the authors -- a selected subset is reported here. The Park90 model with $T_e=T_t$ is chosen as a heritage option for baseline comparison. Park93 and Johnston14 are examined with $T_e=T_v$. The choice of Huo vs Park excitation rates will be examined for selected cases where this has a meaningful impact.

[3] Park 93 has radiative recombination which is not calculated by DPLR

[4] In cases when the references in Johnston's publication do not agree with, or are not the original source of, the rates in Johnston's work, the reference has been corrected in this table.

[5] Park's text (i.e. Park90) is believed to contain a typo. The rate from Park93 is used instead.

[6] Different activation energies are given in Park's 1990 and 1993 publications. DPLR uses the rate from Park's text, even though it is likely incorrect.

[7] Park's text uses the same rate as Park93, but this rate is omitted from DPLR's .chem file due to a typo in Park's text.

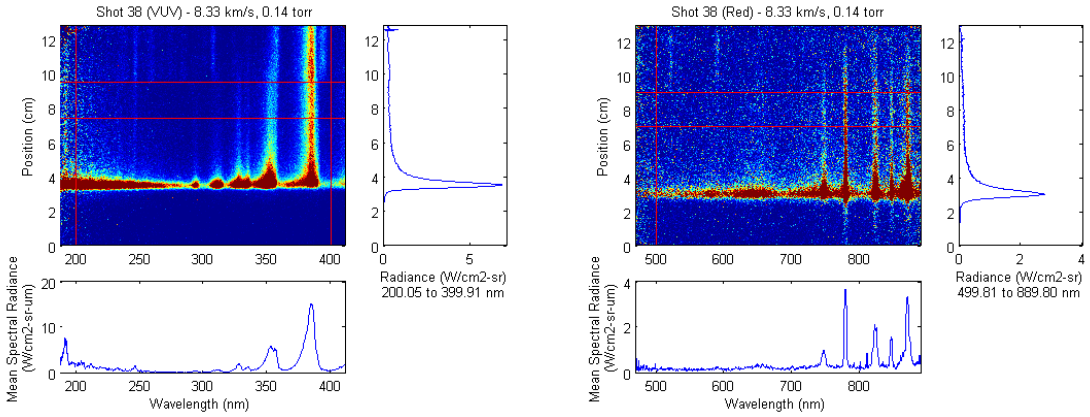

Figure 1. Sample data sets obtained in the EAST facility

IV. Results

The EAST data are obtained in the format of absolute radiance versus position and wavelength. An example data set is shown in Figure 1. The cross-section in the horizontal direction provides a spectral radiance while the vertical direction is the radiance versus position. The radiance versus position displays the non-equilibrium overshoot at the shock front and relaxation toward equilibrium. In order to quantify the non-equilibrium radiance, we have previously defined a metric as the integral of radiance within ±2 cm of the peak radiance.[15, 16] When normalized by the shock tube diameter, this would have units of radiance and is equivalent to the radiance accumulated through 4 cm of the non-equilibrium "zone" when radiation is optically thin. This non-equilibrium metric may also be calculated over spectral radiance data without performing integration over wavelength. In this case it is referred to as the spectral non-equilibrium metric. The spectral non-equilibrium metric is shown in Fig. 2 for one test condition, in order to identify spectral features. The spectral features present are summarized in Table IV.

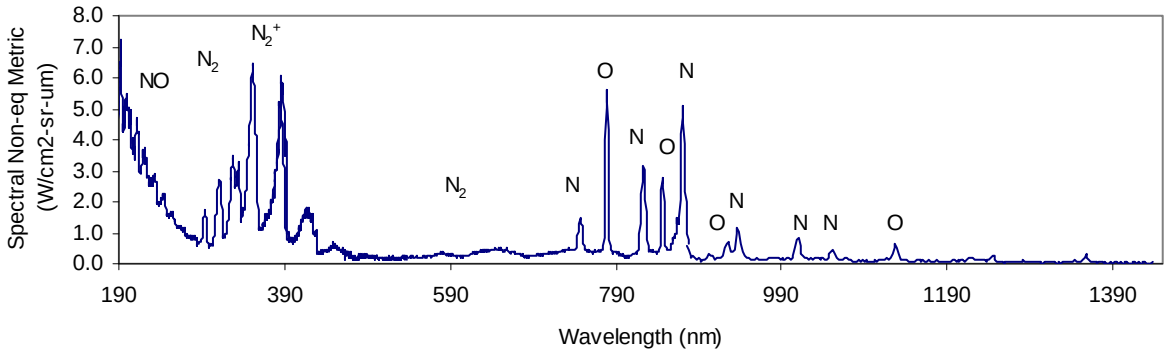

Figure 2. Non-equilibrium spectral metric at 8.33 km/s and 0.14 Torr.

Table IV. Major Spectral Features in this work

Species	Feature	Transition	Major Features or Range (nm)
NO	γ, δ, ε	$(A^2\Sigma^+, C^2\Pi, D^2\Sigma^+) \rightarrow X^2\Pi$	200-300
N_2	2nd Positive	$C^3\Pi \rightarrow B^3\Pi$	337.1 357.7 380.5
	1st Positive	$B^3\Pi \rightarrow A^3\Pi$	500-750
N_2^+	1st Negative	$B^2\Sigma^+_u \rightarrow X^2\Sigma^+_g$	330.8 358.2 391.4

			427.8 470.9
N		3p→3s	744.2 746.8 821.6 862.9 868.0 939.3
	NIR lines	3d→3p	1011.5 1054.0
O		3p→3s	777.2 844.6
	NIR lines	3d→3p	926.6 1128.7

For further analysis, the data is grouped into spectral ranges. The range is determined both by the ranges of individual spectrometers and the spectral features observed. These ranges are summarized in Table V.

Table V. Ranges selected for analysis

Camera	Spectral Range (nm)	Features Included
UV	190-280	NO
	280-320	N_2
	320-370	N2/N2+
UV/Vis	370-500	N2+
Vis/NIR	500-700	N2
	700-890	N,O 3p
NIR	890-1450	N,O 3d

With 7 different spectral regions, 12 different simulation options, and 7 different pressure/tube diameter combinations, the full comparison cannot be presented within this work. Selected comparisons are made instead and are grouped by wavelength range in the following discussion. As discussed above, the Park90 model with $T_e=T_t$ and Park93 and Johnston14 with $T_e=T_v$ are chosen as representative heritage and new models for comparison of spectral features. The radiance versus position is presented with all modeling options at a limited range of pressures.

A. VUV/UV Wavelength (190-500 nm) comparison

The 190-500 nm region primarily consists of molecular features. Because of the lack of atomic features, atomic modeling options, such as excitation rates, have little to no impact on the spectra. Figure 3 shows the comparison of the non-equilibrium spectral metric at 4 of the pressures examined. Radiation features attributed to NO are underpredicted by all models, as are features attributed to the N_2 2^{nd} Positive bands. Prediction of N_2^+ varies significantly with pressure. At the low pressure conditions of 0.01 and 0.05 Torr (not shown), the N_2^+ radiation is significantly overpredicted when using $T_e=T_v$. It is speculated that this is due to the controlling temperature for associative ionization processes in DPLR leading to an overprediction of N_2^+. This phenomenon is currently under investigation. The heritage Park90 ($T_e=T_t$) approach matches the N_2^+ features at 0.01 Torr, but underpredicts radiance at higher pressures. At higher pressures, the N_2^+ radiation becomes more accurately predicted by the $T_e=T_v$ models, agreeing well from 0.14-0.50 Torr, then becoming underpredicted at higher pressure. Some unpredicted CN contamination is observed near 388 nm, particularly in the 4" tube at higher pressures.[17, 18] The differences between Park93 and Johnston models are of little consequence in this range.

a) 0.01 Torr

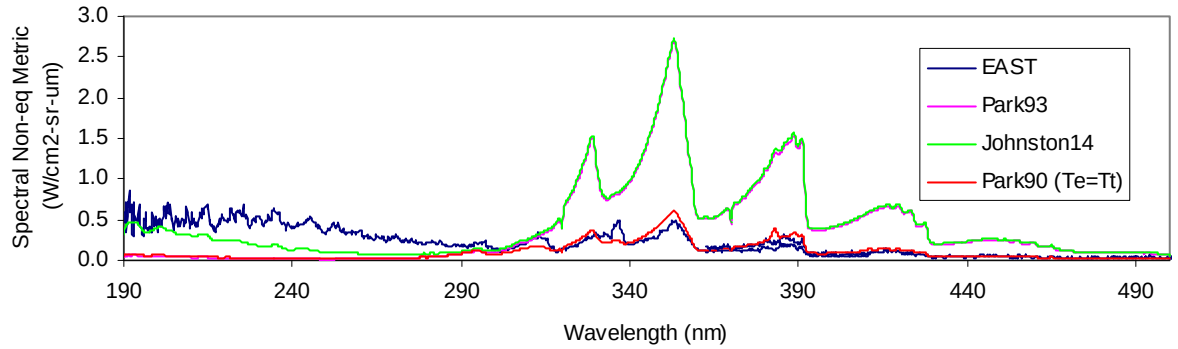

b) 0.14 Torr

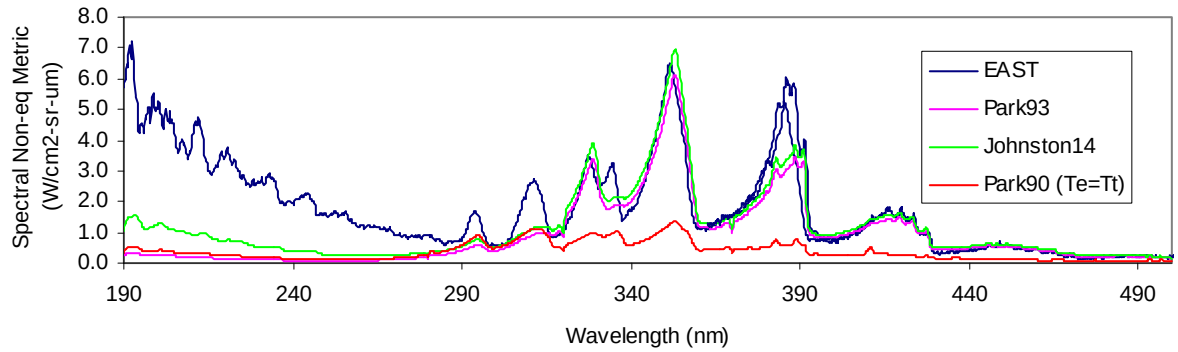

c) 0.30 Torr

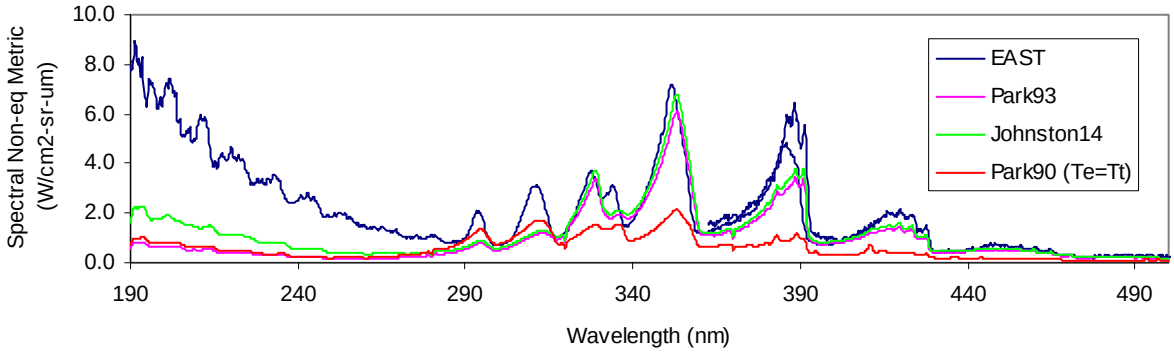

d) 0.70 Torr

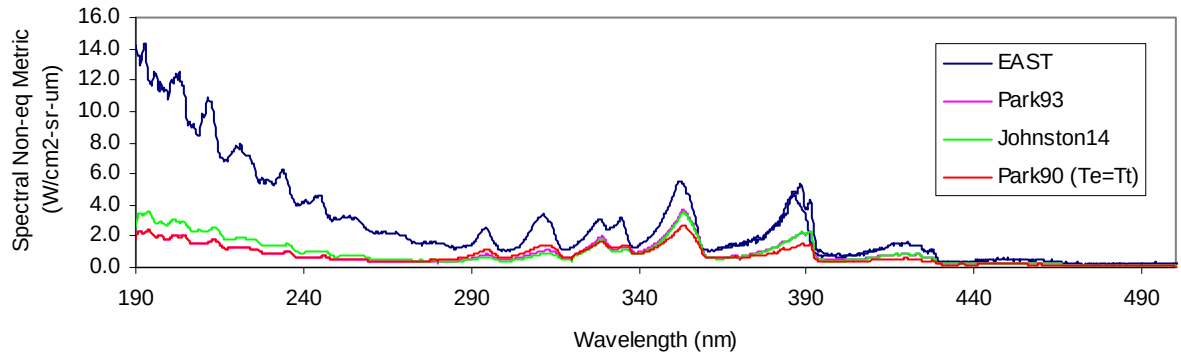

Figure 3. Spectral non-equilibrium metrics from 190-500 nm at four pressures.

The radiance versus position for two of the cases above (0.01 and 0.30 Torr) are shown for the range 320-370 nm in Figure 4, using the 12 different combinations of thermal, chemical and excitation models. The result is insensitive to excitation model because there is no atomic N present in this spectral range. The massive overprediction of N_2^+ radiance discussed above at 0.01 Torr is apparent in all T_e=T_v options. For T_e=T_t, both Park93 and Johnston overpredict substantially. The Park90 model, which showed good agreement in Figure 3(a), is seen not to match the spatial profile and is more sharply peaked than the data. At 0.3 Torr, the T_e=T_t models all underpredict the radiance, while the Johnston model matches the peak signal. The T_e=T_v models, while being close to the spectral non-equilibrium metric (Figure 3), are more peaked in time than the data and do not match the relaxation tail well.

a) 0.01 Torr

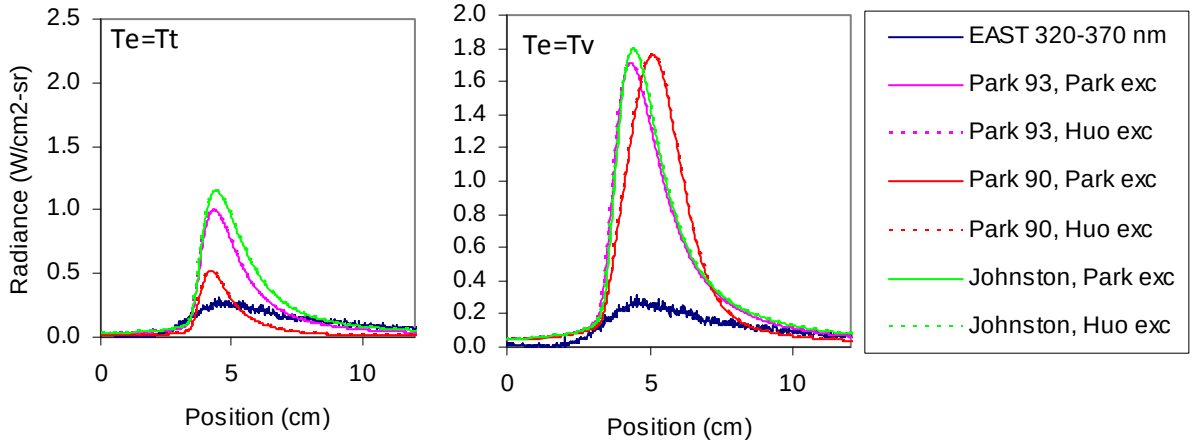

b) 0.30 Torr

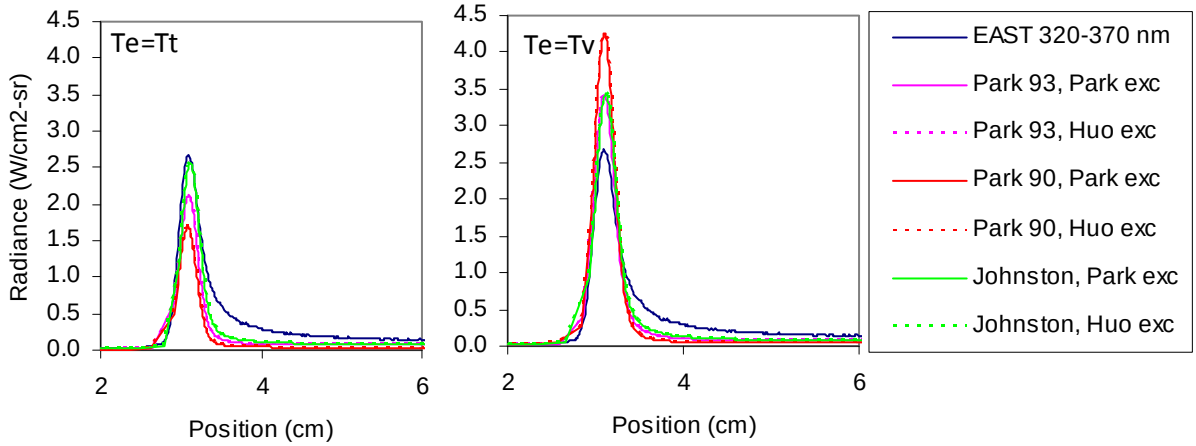

Figure 4. Comparison of radiance from 320-370 nm at pressures of 0.01 Torr (top) and 0.30 Torr (bottom).

B. Vis/Red Wavelength (500-890 nm) comparison

The 500-890 nm region consists of N_2 molecular excitation and atomic 3p transitions. Figure 5 shows the comparison of the non-equilibrium spectral metric in this range at 4 of the pressures examined. In order to aid the comparisons, the integral of the spectral metric is shown as a dotted line. The broad feature from 500-800 nm is attributed to N_2 1st positive radiation and is not predicted by any of the models. Several atomic features are predicted in the 500-700 nm range but are not observed in experiment. These lines generally originate from 5s and higher states of N, indicating the density of upper states is overpredicted. Lines at 777 and 845 nm are attributed to

3s states of O. The 777 nm line is underpredicted by $T_e=T_v$ models at all conditions, while the Park 90 ($T_e=T_t$) model displays a fair match from 0.14-0.50 Torr, but underpredicts at high and low pressure. The agreement to the 845 nm line is similar to the 777 nm line at pressures above 0.14 Torr, but inverts at lower pressure, where the line is well matched by Park90 ($T_e=T_t$) but overpredicted by the $T_e=T_v$ models. The 845 nm line is just slightly higher in energy than the 777 nm line, and the disagreement indicates errors in either the QSS prediction or the electronic temperature input to NEQAIR. The atomic N lines are generally overpredicted at the lowest pressure, but matched well from 0.05-0.50 Torr. At 0.70 Torr, the N lines are underpredicted by the Te=Tv models but matched by Park90 ($T_e=T_t$).

The radiance from 700-890 nm versus position is shown in Figure 6 for pressures of 0.05 and 0.50 Torr. Regardless of temperature model, the Huo excitation underpredicts the radiance profile significantly. For the Park90 kinetics, the Huo excitation produces an extended decay in radiance . This is attributed to a slow equilibration of N^+ within the Park90 model, due to the absence of N_2/N charge exchange, coupled with a slow interaction between ground and excited states in the Huo model, which favors a Saha-like distribution. Given the poor agreement to experiment, the Huo results will not be discussed further for this wavelength range. At 0.05 Torr, cases with Te=Tt underpredict the radiance or do not follow the decay profile. Of the $T_e=T_v$ solutions, the Johnston model with Park excitation shows good apparent agreement with the data. Spectral data, however, show that the Johnston model overpredicts N atom and underpredicts O atom, to the extent that the total radiance balances. The Park93 model underpredicts the initial radiance while Park90 overpredicts. The Park93 results are observed to better predict the N atom radiance in comparison to Johnston. At higher pressure (0.5 Torr) the differences between $T_e=T_t$ and $T_e=T_v$ become less distinguished, indicating that the extent of thermal non-equilibrium is diminishing at higher pressure. The Park90 model overpredicts radiance with longer decays while the Johnston and Park93 rates yield a narrower peak. Examination of the spectral data show that the N atom intensities are well matched and the underprediction is mainly due to the O atom and underlying N_2 molecular radiation.

a) 0.01 Torr

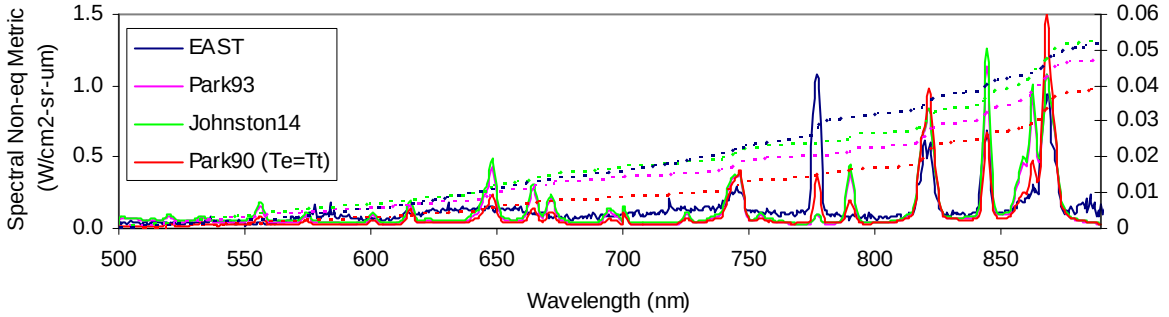

b) 0.14 Torr

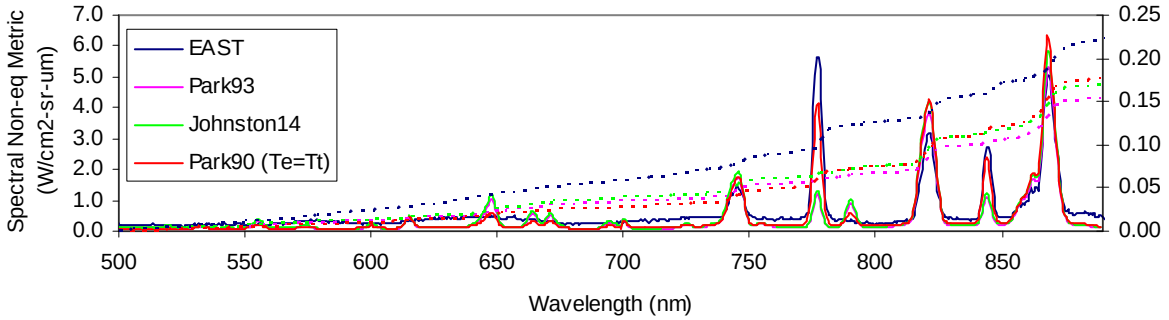

c) 0.30 Torr

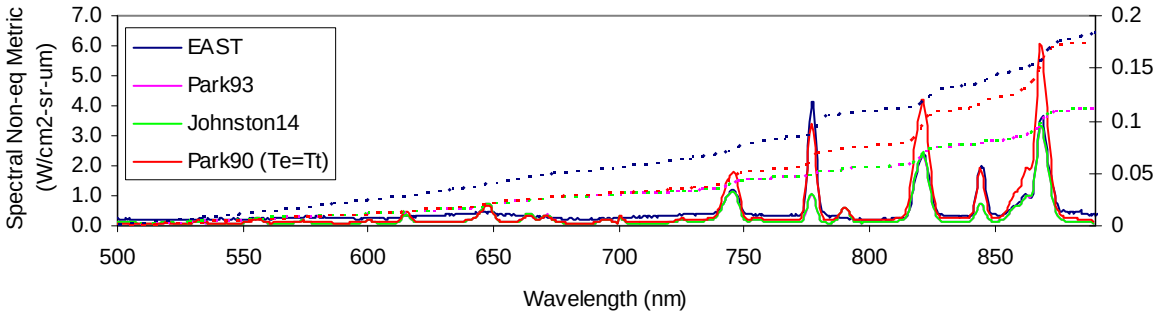

d) 0.70 Torr

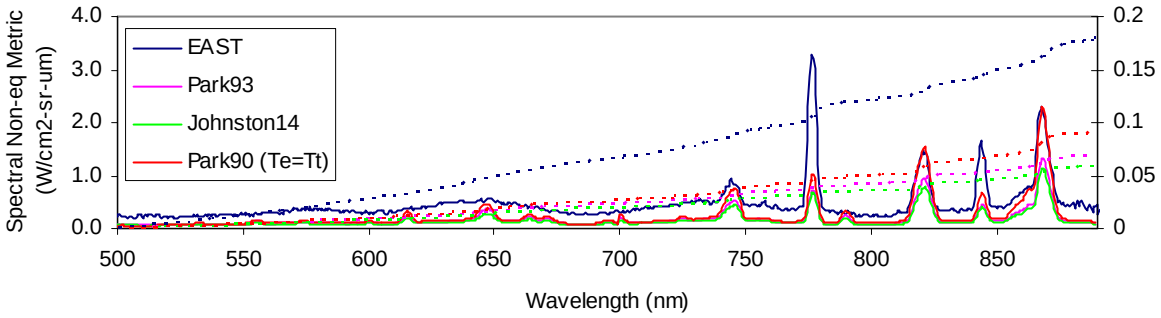

Figure 5. Spectral non-equilibrium metrics from 500-890 nm.

a) 0.05 Torr, 8.87 km/s

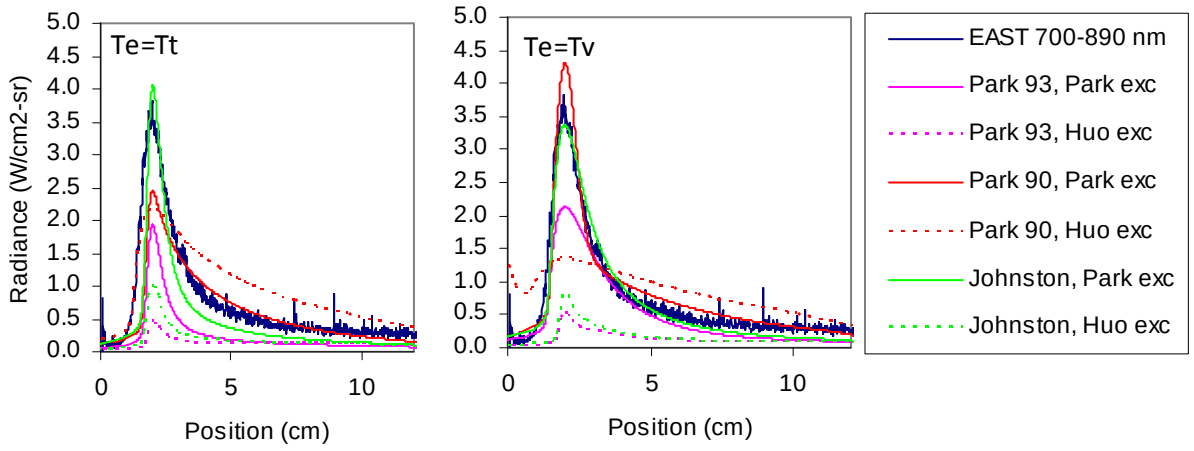

b) 0.50 Torr, 7.71 km/s

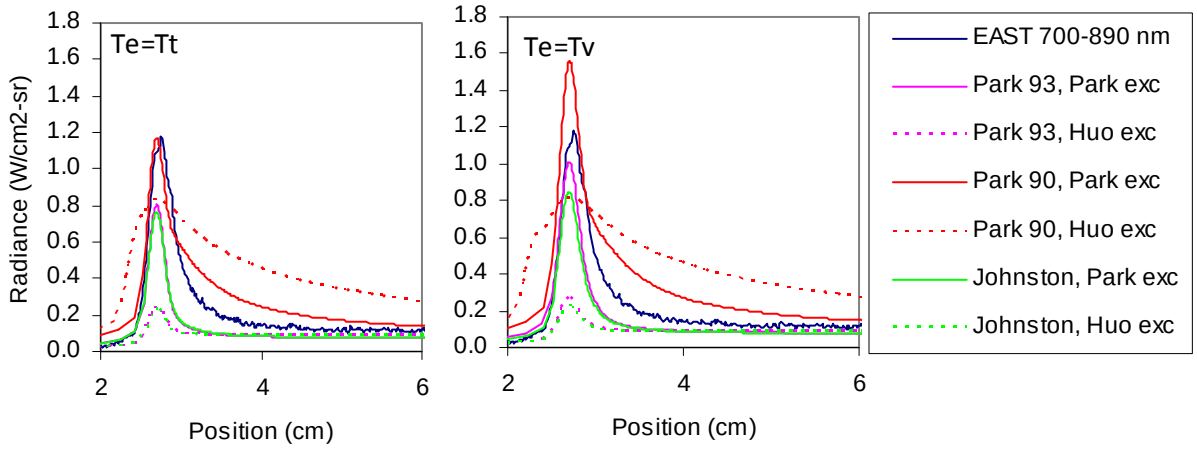

Figure 6. Radiance versus position from 700-890 nm.

C. IR Wavelength (890-1450 nm) comparison

The 890-1450 nm region consists primarily of atomic 3d transitions, though one N 3p transition of significant intensity is within this range. In this range, the Park excitation model produces a substantial overprediction. The comparisons presented in Figure 7 therefore use the Huo excitation rates. The integrated radiance is matched reasonably well by all models at 0.01 Torr, Park93/Johnston at 0.14 and 0.3 Torr and Park90 at 0.7 Torr. However, the strengths of individual features are not matched. Three lines attributable to atomic O are substantially overpredicted by all models at all pressures. This compensates under prediction in other areas such that the integrated intensity agrees. The one line attributed to the N 3p state at 939 nm is under predicted with the Huo excitation rates for Park93/Johnston, but becomes overpredicted by Park90 above 0.05 Torr. The Park excitation rates (not shown) predict this particular line better, consistent with the observations from 700-890 nm. However, the Park excitation overpredicts the intensity of the 3d states of N substantially.

a) 0.01 Torr

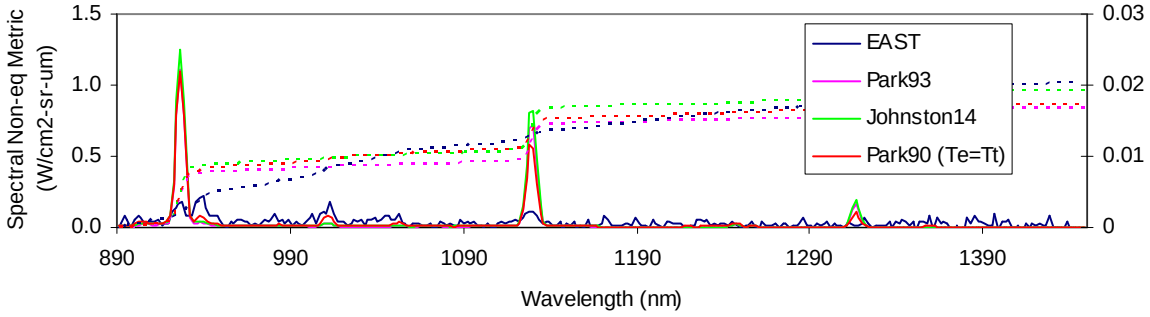

b) 0.14 Torr

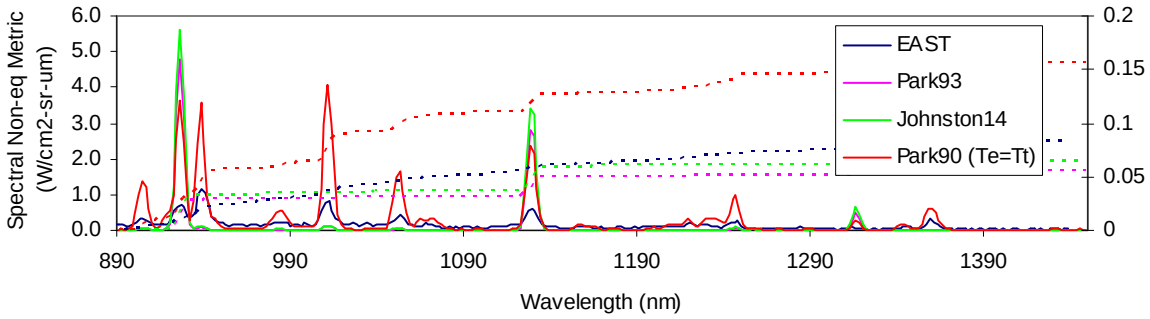

c) 0.30 Torr

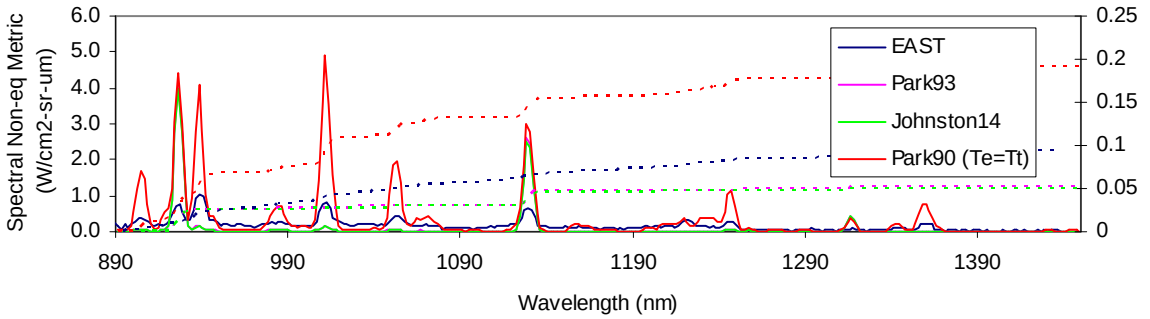

d) 0.70 Torr

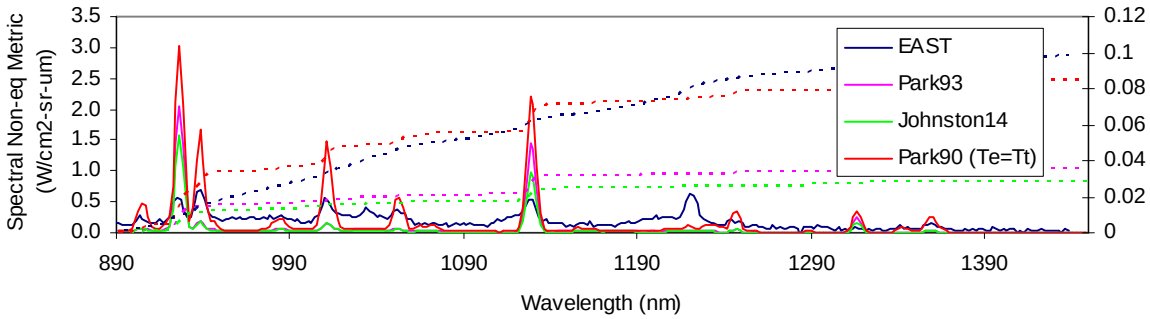

Figure 7. Spectral non-equilibrium metrics from 890-1450 nm.

The comparison of relaxation is selected at representative pressures of 0.01 and 0.30 Torr in Figure 8. Substantial overprediction at both pressures is observed with the Park excitations due to excessive radiation for 3d states. Some of the Huo excitation curves appear to agree well with the radiance curve due to offsetting errors in N and O radiation intensities. At low pressure, the curves are more sharply peaked for T_e=T_t models, while the T_e=T_v trend is more consistent with experiment.

a) 0.01 Torr, 8.57 km/s

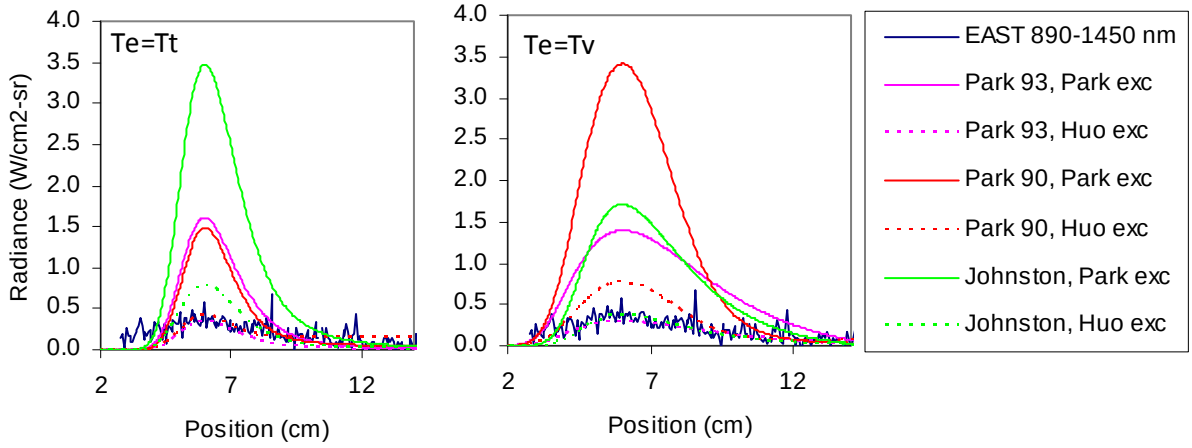

b) 0.30 Torr, 8.09 km/s

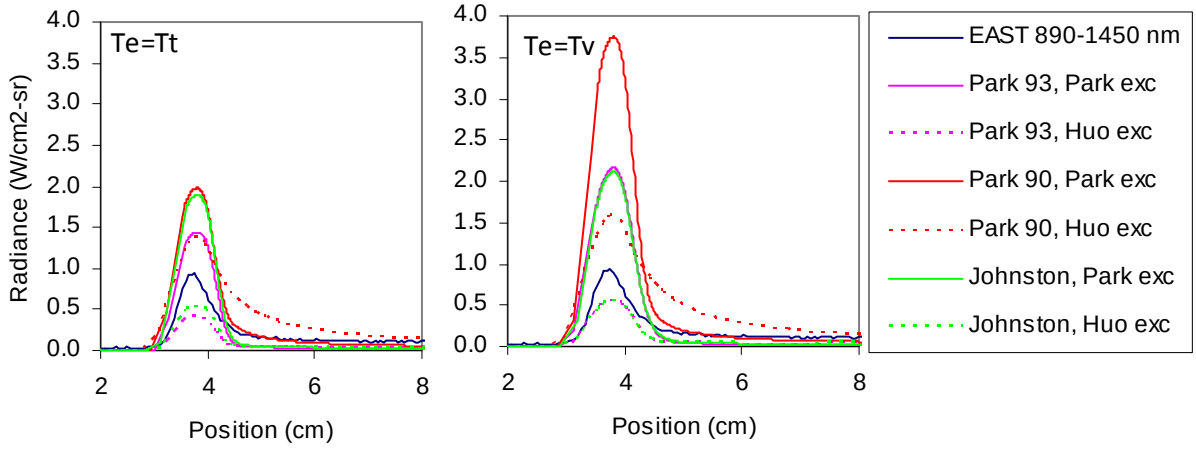

Figure 8. Radiance versus position from 890-1450 nm for two selected tests.

V. Summary

A comparison of non-equilibrium radiance at shock speeds from 7-9 km/s and pressures from 0.01-0.70 Torr has been presented. The vast amount of data obtained meant that only a subset could be presented in this work. Comparisons are presented in terms of a non-equilibrium spectral metric, which is the integral of radiance over a 4 cm length, 2 cm in front of the shock to 2 cm behind the shock, normalized by shock tube diameter. These results are compared against predictions by the DPLR and NEQAIR codes using twelve different modeling options by varying the two-temperature model, reaction kinetics and internal excitation rates.

The comparison focuses on radiation from NO, N_2, N_2^+ and atomic N and O. The NO and N_2 radiation is underpredicted by all models at all conditions. N_2^+ radiation is overpredicted at low pressure when T_e=T_v, and this is attributed to the controlling temperature for associative ionization reactions. N_2^+ radiation is predicted well at low pressure with the heritage model (Park 90 and T_e=T_t) but is better matched by either Park93 or Johnston kinetics and T_e=T_v at intermediate pressures (0.14-0.50 Torr). At higher pressures, the N_2^+ non-equilibrium is underpredicted by all models. Atomic line radiation predictions are mixed. The lowest energy states of N (3p) are predicted well from

0.05-0.50 Torr when $T_e=T_v$ is employed. The 3p states of atomic O are overpredicted by the $T_e=T_v$ models but predicted well at intermediate pressure ranges by the heritage model. Higher energy N and O lines, however, are overpredicted. The excitation rates recommended by Huo and implemented in NEQAIR were found to underpredict most atomic features. This could be due to the way in which states are combined within NEQAIR, but these rates are not recommended for use based on the present comparison. The present work suggests that the best radiation modeling options currently are to use $T_e=T_v$ with either Park93 or Johnston kinetics and Park excitation rates. The final paper will examine modeling discrepancies in further detail and suggest updates to modeling practice that may improve comparison over a wider range of conditions.

Acknowledgments

The authors would like to thank NASA's MPCV Aerosciences Program and Entry Systems Modeling (ESM) project. Brett Cruden and Aaron Brandis are supported through contract NNA15BB15C to AMA Inc.

References

1. Brandis, A. M., Johnston, C. O., Cruden, B. A., Prabhu, D., and Bose, D., "Uncertainty Analysis and Validation of Radiation Measurements for Earth Reentry," *Journal of Thermophysics and Heat Transfer,* Vol. 29, No. 2, 2015, pp. 209-221.
2. Cruden , B. A., "Absolute Radiation Measurements in Earth and Mars Entry Conditions," RTO-EN-AVT-218, 2014.
3. Wright, M. W., White, T., and Mangini, N., "Data Parallel Line Relaxation (DPLR) Code User Manual Acadia – Version 4.01.1," NASA/TM-2009-215388, October 2009.
4. Cruden , B. A., and Brandis, A. M., "Updates to the NEQAIR Radiation Solver," *Radiation in High Temperature Gases*. St. Andrews, UK, 2014.
5. Park, C., *Nonequilibrium Hypersonic Aerothermodynamics*, New York: John Wiley & Sons, 1990.
6. Park, C., "Review of chemical-kinetic problems of future NASA missions. I - Earth entries," *Journal of Thermophysics and Heat Transfer,* Vol. 7, No. 3, 1993, pp. 385-398.
7. Johnston, C. O., "Study of Aerothermodynamic Modeling Issues Relevant to High-Speed Sample Return Vehicles," VKI 2013-AVT-218.
8. Huo, W. M., Liu, Y., Panesi, M., Wray, A., and Carbon, D. F., "Electron-Impact Excitation Cross Sections for Modeling Non-Equilibrium Gas," AIAA Paper 2015-1896.
9. Gnoffo, P. A., Gupta, R. N., and Shinn, J. L., "Conservation Equations and Physical Models for Hypersonic Air Flows in Thermal and Chemical Nonequilibrium," NASA-TP-2867, Feb 1989.
10. Johnston, C. O., and Brandis, A. M., "Modeling of nonequilibrium CO Fourth-Positive and CN Violet emission in CO2–N2 gases," *Journal of Quantitative Spectroscopy and Radiative Transfer,* Vol. 149, 2014, pp. 303-317.
11. Fujita, K., Yamada, T., and Ishii, N., "Impact of Ablation Gas Kinetics on Hyperbolic Entry Radiative Heating," 2006.
12. Bose, D., and Candler, G. V., "Thermal rate constants of the O-2+ N-> NO+ O reaction based on the (2) A'and (4) A'potential-energy surfaces," *Journal of Chemical Physics,* Vol. 107, No. 16, 1997, pp. 6136-6145.
13. Bourdon, A., and Vervisch, P., "Study of a low-pressure nitrogen plasma boundary layer over a metallic plate," *Physics of Plasmas (1994-present),* Vol. 4, No. 11, 1997, pp. 4144-4157.
14. Teulet, P., Gonzalez, J., Mercado-Cabrera, A., Cressault, Y., and Gleizes, A., "One-dimensional hydro-kinetic modelling of the decaying arc in air–PA66–copper mixtures: I. Chemical kinetics, thermodynamics, transport and radiative properties," *Journal of Physics D: Applied Physics,* Vol. 42, No. 17, 2009, p. 175201.
15. Cruden, B. A., "Radiance Measurement for Low Density Mars Entry," AIAA Paper 2012-2742.
16. Brandis, A. M., Johnston, C. O., Cruden, B. A., and Prabhu, D. K., "Investigation of Nonequilibrium Radiation for Mars Entry," AIAA Paper 2013-1055.
17. Cruden, B. A., Martinez, R., Grinstead, J. H., and Olejniczak, J., "Simultaneous Vacuum Ultraviolet through Near IR Absolute Radiation Measurement with Spatiotemporal Resolution in an Electric Arc Shock Tube," AIAA Paper 2009-4240.
18. Bose, D., McCorkle, E., Bogdanoff, D., and Gary A. Allen, J., "Comparisons of Air Radiation Model with Shock Tube Measurements," AIAA 2009-1030.